

## Effect of Interface Momentum Distribution on the Stability in a Porous-Fluid System

P. Hu and Q. Li<sup>†</sup>

*School of Energy and Power Engineering, Northeast Electric Power University, Jilin 132012, PR China*

<sup>†</sup>Corresponding Author Email: [liqi\\_1015@163.com](mailto:liqi_1015@163.com)

(Received June 2, 2019; accepted October 15, 2019)

### ABSTRACT

We numerically investigate the linear instability problem of Poiseuille flow in a channel partially filled with a porous medium on the bottom side. We are primarily interested in the influence of the interface momentum distribution including stress continuity and jump interface conditions. A spectral collocation method is applied in solving the fully coupled instability problem arising from the adjacent porous and free channel flows. The results show that the “interface stress coefficient” in a negative range has a larger effect on the trajectory of the eigenvalues than that in the positive range, especially the most unstable mode. Moreover, with a low permeability in the porous region, the interface momentum distribution has less effect on the stability of core flow. And when the “interface stress coefficient” is equal to its minimum negative value, the flow passing through the channel is at its most stable state. If the “interface stress coefficient” varies in a positive range, the degree of fluid stability is predicted to slightly diminish due to stress continuity condition at the interface.

**Keywords:** Porous layer; Linear stability; Interface momentum distribution; Poiseuille flow.

### NOMENCLATURE

$c$	dimensionless complex phase speed	$u_m$	the mean velocity
$c_r$	dimensionless real part of phase speed	$\langle u \rangle$	volume-averaged velocity in the porous matrix, dimensionless
$c_i$	dimensionless imaginary part of phase speed	$\tilde{u}$	velocity perturbation amplitudes in the $y$ direction
$D$	$d/dy$	$U$	dimensionless laminar profile in the unobstructed portion of the channels
$Da$	Darcy number	$\alpha$	streamwise wave number
$h_p$	half height of porous layer	$\mu$	dynamic viscosity
$h_f$	half height of open fluid layer	$\rho$	density
$k$	permeability of porous media	$\varepsilon$	porosity of porous medium
$p$	pressure of porous media, dimensionless	$\sigma$	nondimensional permeability
$\bar{p}$	pressure perturbation amplitudes in the $y$ direction	$\tau$	interface stress coefficient
$Re$	Reynolds number		
$Re_c$	critical Reynolds number		

### 1. INTRODUCTION

Flow in a porous–fluid system has numerous industrial and geotechnical applications and consequently has been given much attention in the literature, such as hydrogeological systems including ground water, oil reservoirs (Berkowitz, 2002; Coronado & Jetzabeth Ramirez-Sabag, 2008), and some industry applications including drying systems (Pirasteh *et al.*, 2014), filtration processes (Hanspal *et al.*, 2006) and solar air heaters (Singh &

Dhiman, 2016). The instability analysis of free fluid region and fluid saturated porous region in a porous–fluid mechanics has recently been a major problem of many researches. By investigating the stability of such a system involving fluid flows through or over porous materials, its critical  $Re$  number at given conditions can be obtained, or give a prediction for a certain porous media system achieving its stable or unstable state by varying permeability, momentum transfer at the interface, etc. Although the previous researches involve the

stability study of channel flows, the mathematic models used for describing a fully developed laminar flow in a homogeneous porous region or at the interface may not be consistent. Beavers and Joseph (1967) originally proposed the mathematic model at the interface for a porous-fluid channel. They put forward a slip velocity concept at the interface between the free fluid domain and porous domain. Then, Beavers *et al.* (1973) presented a two dimensional Poiseuille flow instability analysis applying the proposed interface condition and Darcy model in porous layer. They showed that in one channel having a porous wall, the porous wall is able to decrease the critical Reynolds number comparing with impermeable wall, and found the theoretical predictions based on the proposed condition were in accord with experiment data they performed. Chang *et al.* (2006) studied a Poiseuille flow stability problem for a free fluid layer overlying a saturated porous layer using Darcy model with the slip velocity boundary condition, and found out a tri-modal form in the neutral curves. These three kinds of modes generally have different characteristics of stability, and are caused by Poiseuille flow's shear stress in a fluid region. Still, Darcy model fails to figure out boundary layers that may lead to the velocity discontinuity at the interface. Therefore, Brinkman-extended Darcy model was applied in order to solve this problem by Vafai and Kim (1990) and Neale and Nader (1974), who support the Brinkman-extended Darcy model that the shear stress as well as the velocity at the interface should be continuous. With the sophisticated volume averaging method, Ochoa-Tapia and Whitaker (1995a, b) established one model that the shear stress should be discontinuous while the velocity should be continuous, and using that interface conditions and the governing equations proposed by Whitaker (1996), Tilton and Cortezzi (2006) presented the three-dimensional Poiseuille flow stability problem in a porous-fluid channel with two porous walls on both sides. They discovered that with decreasing the wall permeability at a very small value may greatly decrease the channel flow's stability comparing the channel flow having impermeable walls. Moreover, they continued to analyze the effects of the porosity, permeability, the interface stress coefficient, and the porous layers' height, on the symmetric flow's stability with two porous walls on both sides of a channel (Tilton & Cortezzi 2008). Li *et al.* (2014) also applying the equations of Whitaker (1996) for the porous region with the interface conditions of Ochoa-Tapia and Whitaker (1995a, b), performed a coupled flow instability analysis for a porous layer placed in the middle of a channel, mainly focused on the influence of the porous filling ratio. Then, Dai *et al.* (2015) further performed a linear Poiseuille flow instability investigation for the fluid saturated multilayer porous media inserted in a channel, mainly focused on the influence of porous layer number. There were two ways for increasing the number of porous layers considered: constant Reynolds number condition and constant porous filling ratio condition. They observed that both conditions have a less stability as the number of

porous layers increases. At the same number of porous layers, the value of critical Reynolds number at constant porous filling ratio condition is much less than that at constant Reynolds number condition. Avramenko *et al.* (2005) took into account both linear Darcy and quadratic Forchheimer drag terms in the porous medium. The obtained results indicate that both linear and quadratic drag terms increase the critical value of the Reynolds number. Liu *et al.* (2008) performed the instability of Poiseuille flow in a fluid-porous system. They investigated the influence of the depth ratio and the Darcy number on the instability of the system were, and also compared thoroughly the characteristics of the instability of Brinkman's model with that of Darcy's model. Rosti *et al.* (2015) investigated a turbulent channel flow over porous walls using direct numerical simulations (DNS). They found that the permeability plays a major role in determining the response of the channel flow to the permeable wall even it is very small. Tryggvason *et al.* (2016) and Ma *et al.* (2016) also used direct simulation and data driven method but to model bubbly flows. Barletta and Antonio (2016) analysed the linear stability of the basic two-dimensional mixed convection. The growth rate and the angular frequency of the perturbations were evaluated numerically. Wedin and Cherubini (2016) used the asymptotic suction boundary layer (ASBL) for investigating two permeability models which are the Darcy and the Forchheimer models.

From above references it is noted that although the previous researches involve the stability study of porous channel flows, the mathematic models used for describing a fully developed laminar flow in a homogeneous porous region or at the interface may not be consistent. Few studies investigate the effect of the interface momentum distribution on the linear stability characteristics including the velocity perturbation, the Orr-Sommerfeld spectrum and the critical Reynolds number, and to the best of our knowledge, the linear stability problem in an asymmetric porous-fluid system has not been studied yet. This study aims to indicate the impact of the interface momentum distribution on the linear stability problem in an asymmetric porous-fluid channel which is constructed by a bottom porous layer. In order to know how the surface characteristics of the porous material in the transition layer influences a coupled asymmetric porous-fluid flow stability, first, the effect of permeability with fixed interface momentum distribution coefficient  $\tau = 0.0$  is studied indicating a stress continuity interface condition, and then the stress jump effects of varying in interface stress coefficient  $\tau = -1.0-1.5$  on the velocity perturbation, the Orr-Sommerfeld spectrum and the critical Reynolds number are discussed.

## 2. GOVERNING EQUATIONS

The present coupled channel geometry considered in the paper is shown in Fig. 1. In Fig. 1, the channel is restricted by impermeable walls. A

porous layer which is rigid and homogeneous is placed on the bottom side of the channel paralleled to the impermeable walls. Thus, the channel is divided into two layers that are a porous layer below and a free fluid layer above. The two layers' heights are defined as  $2h_f$  and  $2h_p$ , respectively. We consider a two dimensional laminar flow, and the fluid is incompressible, viscous and Newtonian. Both the channel region and the porous region hold a laminar, fully developed flow driven by the uniform pressure gradient just in x-direction.

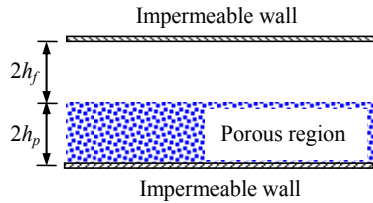


**Fig. 1. Coupled flow geometry considered.**

In the fluid region, the governing equation is Navier-Stokes model, while in the porous region, the governing equation is the model proposed by Whitaker (1996). A length scale can be defined as the half-height in fluid region,  $h_f$ , a time scale is the ratio of the half-height to the mean velocity in the free fluid layer,  $h_f/u_m$ , and the dimensionless pressure is  $p/\rho u_m^2$ . The formulas for the fluid domain and the porous domain then can be nondimensional as follows:

$$\frac{\partial \mathbf{u}}{\partial t} + \mathbf{u} \cdot \nabla \mathbf{u} = -\nabla p + \frac{1}{Re} \nabla^2 \mathbf{u}, \quad (1)$$

$$\nabla \cdot \mathbf{u} = 0, \quad (2)$$

$$\frac{1}{\varepsilon} \frac{\partial \langle \mathbf{u} \rangle}{\partial t} = -\nabla \langle p \rangle^f + \frac{1}{\varepsilon Re} \nabla^2 \langle \mathbf{u} \rangle - \frac{1}{\sigma^2 Re} \langle \mathbf{u} \rangle, \quad (3)$$

$$\nabla \cdot \langle \mathbf{u} \rangle = 0. \quad (4)$$

In above equations, the symbols  $\mathbf{u}=[u \ v]^T$ ,  $\varepsilon$  and  $p$  represent the fluid velocity in the fluid region or porous region, porosity and pressure of porous medium. In Eq. (3), the symbols  $\langle \rangle$  and  $\langle \rangle^f$  represent the superficial volume average and the intrinsic volume average, in a relationship of  $\langle \rangle = \varepsilon \langle \rangle^f$ . The last two terms in Eq. (3) on the right side in turn are Brinkman term, which is only important near the interfaces in the Brinkman boundary layers, Darcy term, which refers to a volume-averaged viscous drag. A Reynolds number is given as the form of  $Re = \rho u_m h_f / \mu$  for the fluid flow in the free fluid layer, in which  $u_m$ ,  $\mu$  and  $\rho$  symbolize mean velocity in the free channel, viscosity, and density of the fluid. The symbol  $\sigma = \sqrt{k} / h_f = (Da)^{1/2}$  ( $k$  refers to the dimensional penetrability of the porous material) indicates the dimensionless permeability in the porous region.

In the present paper, we have restricted the study to channel flows for not considering the inertial

influence both in porous region and at the interface, and also ignored the convective terms in porous region (Tilton & Cortelezzi 2006).

## 2.1 Basic Flow

In this study, we assume a fully developed laminar flow in the free fluid layer and porous layer is driven by a uniform pressure gradient only in x-direction,  $dp/dx$ . Therefore, the dimensionless momentum equation for the open channel fluid layer becomes

$$\frac{d^2 u}{dy^2} = Re \frac{dp}{dx}. \quad (5)$$

The momentum equation for the porous layer becomes:

$$\frac{1}{\varepsilon} \frac{d^2 \langle u \rangle}{dy^2} - \frac{1}{\sigma^2} \langle u \rangle = Re \frac{d \langle p \rangle^f}{dx}. \quad (6)$$

The boundary conditions at the impermeable walls are

$$u = 0, \quad \langle u \rangle = 0. \quad (7)$$

Ignoring the inertial effect in the momentum transfer process, but taking account of the momentum jump, the interface conditions are (Ochoa-Tapia and Whitaker 1995a, b):

$$\langle p \rangle^f = p, \quad \langle \mathbf{u} \rangle = \mathbf{u}, \quad \frac{1}{\varepsilon} \frac{\partial \langle \mathbf{u} \rangle}{\partial y} - \frac{\partial \mathbf{u}}{\partial y} = -\frac{\tau}{\sigma} \mathbf{u}. \quad (8)$$

$\tau$  indicates the interface distribution of momentum in a porous-fluid system, which is called the interface stress coefficient. Ochoa-Tapia and Whitaker (1995b) found that the interface stress coefficient  $\tau$  is roughly between  $-1.0$  and  $1.5$ . The value of  $\tau$  mainly depends on the characteristics of surface machining at the interface and the porous structures varying in the transition layer. Additionally, it must usually be determined experimentally.

From the above equations, we can get the solutions for the laminar velocity in the free fluid layer and in the porous layer as:

$$U = \frac{1}{1/3 + c_2} (y^2 + c_1 y + c_2) \quad y \in (-1, 1), \quad (9)$$

$$\langle U \rangle = c_3 e^{\frac{\sqrt{\varepsilon}}{\sigma} y} + c_4 e^{-\frac{\sqrt{\varepsilon}}{\sigma} y} - \frac{\sigma^2}{1/3 + c_2} y \quad y \in (-h_p/h_f, h_p/h_f). \quad (10)$$

Where the constant coefficients  $c_1$ ,  $c_2$ ,  $c_3$ ,  $c_4$  in Eqs. (9) and (10) are achieved through assembling all the interface as well as boundary requirements (7) and (8).

Figure 2 shows the basic flow simulation results both in porous layer and free fluid layer when  $\sigma = 0.002$ ,  $\varepsilon = 0.6$ ,  $h_f/h_p = 1.0$ ,  $\tau = 0.0$ . In Fig. 2, it is noted that the fluid maximum velocity is 1.49884 in the free channel layer; the interface velocity is 0.00464; the Darcy velocity in porous medium is  $5.98608 \times 10^{-6}$ . The marked velocity values in the

three different regions decrease about at most 6 orders of magnitude along  $y$ -direction if inserting the porous wall. In order to known clearly how certain parameters affect the velocity profiles, figure 3 gives the velocity profiles in each region, especially at the interface by changing the permeability  $\sigma$  and the interface stress coefficient  $\tau$ . It is observed that at a lower permeability  $\sigma$ , changing  $\tau$  has an ignoring effect on velocity distribution. Increasing  $\sigma$  increases the boundary layer near the interface between the porous and fluid regions, leads to a less steep velocity gradient near the interface since there is a less sharp and sudden variation of permeability  $\sigma$  at the interface in a porous-fluid channel. Moreover, at a fixed permeability  $\sigma$ , the interface velocity decreases as  $\tau$  increases, and changing the values of  $\tau$  within a scope of negative range may make an obvious different velocity profile near the interface than the situation of changing the values of  $\tau$  within a scope of positive range. This conclusion can also be reflected in part 3.

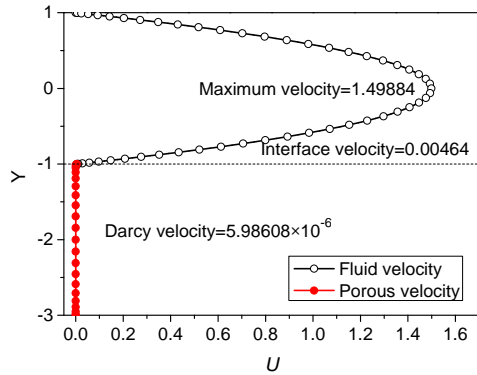


Fig. 2. Velocity profiles at  $Re=2000$ ,  $\varepsilon = 0.6$ ,  $\sigma = 0.002$ ,  $h_f/h_p = 1.0$ ,  $\tau = 0.0$ .

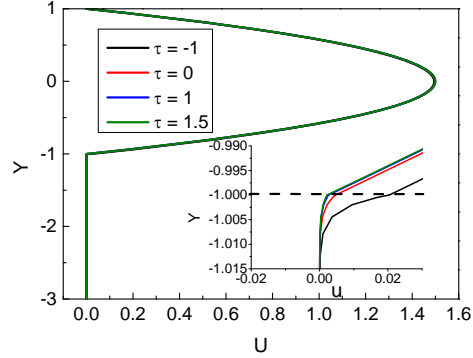
## 2.2 Perturbation Equations

Considering two-dimensional perturbation equations, the wave-like fluid perturbations in both free fluid region and porous region can be expected to have identical phase speeds and wave numbers,

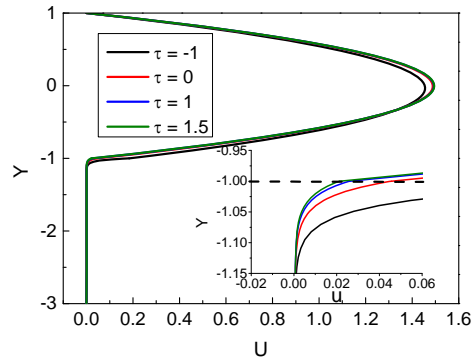
$$\begin{cases} \hat{\mathbf{u}} = \tilde{\mathbf{u}}_f(y)e^{i(\alpha x - \alpha ct)}, \\ \langle \hat{\mathbf{u}} \rangle = \tilde{\mathbf{u}}_p(y)e^{i(\alpha x - \alpha ct)}, \\ \hat{p} = \tilde{p}_f(y)e^{i(\alpha x - \alpha ct)}, \\ \langle \hat{p} \rangle^f = \tilde{p}_p(y)e^{i(\alpha x - \alpha ct)}. \end{cases} \quad (11)$$

Where  $\tilde{\mathbf{u}}_p$  or  $\tilde{\mathbf{u}}_f$  and  $\tilde{p}_p$  or  $\tilde{p}_f$  are the porous or free fluid velocity and pressure perturbation amplitudes in  $y$ -direction.  $\alpha$  represents the streamwise wave number, and  $c = c_r + ic_i$  represents the complex phase speed, in which  $c_r$  and  $c_i$  are the real part and imaginary part, respectively. The perturbed base flow then can be shown in Eq. (12) where  $U$  means the basic flow in the free channel,  $\langle U \rangle$  means the laminar profile in the porous layer:

$$\begin{cases} \mathbf{u} = U(y) + \hat{\mathbf{u}}, \\ \langle \mathbf{u} \rangle = \langle U \rangle(y) + \langle \hat{\mathbf{u}} \rangle, \\ p = p(x) + \hat{p}, \\ \langle p \rangle^f = p(x) + \langle \hat{p} \rangle^f. \end{cases} \quad (12)$$



(a)  $\sigma = 0.002$



(b)  $\sigma = 0.02$

Fig. 3. Velocity profiles with changing  $\tau$  under different  $\sigma$  at  $Re=2000$ ,  $\varepsilon = 0.6$ ,  $h_f/h_p = 1.0$ , and their corresponding enlarged figures at the interface.

Substitute the formula (12) into the Eqs. (1)-(4), the resulting perturbation equation for the free fluid layer can be derived as (in which both labels "D" and " " mean  $d/dy$ ):

$$\left[ (U - c)(D^2 - \alpha^2) - U'' - \frac{1}{i\alpha Re}(D^2 - \alpha^2)^2 \right] \tilde{v}_f(y) = 0. \quad (13)$$

While the flow stability model for the porous layer can be deduced as:

$$\left[ -c(D^2 - \alpha^2) - \frac{1}{i\alpha Re}(D^2 - \alpha^2)^2 + \frac{\varepsilon}{i\alpha Re\sigma^2}(D^2 - \alpha^2) \right] \tilde{v}_p(y) = 0. \quad (14)$$

By taking the momentum transfer Eq. (8), the interface boundary conditions coupling,  $\tilde{v}_f$ , and  $\tilde{v}_p$  can be deduced as follows (Tilton and Cortezzi 2006, 2008):

$$\tilde{v}_f = \tilde{v}_p, \frac{d\tilde{v}_f}{dy} = \frac{d\tilde{v}_p}{dy}, -\frac{\sigma}{\varepsilon} \frac{d^2\tilde{v}_p}{dy^2} + \sigma \frac{d^2\tilde{v}_f}{dy^2} = \tau \frac{d\tilde{v}_f}{dy}, \quad (15)$$

$$\left[ \left( \frac{1}{\varepsilon} - 1 \right) \left( i\alpha c - \frac{\alpha^2}{Re} \right) - \frac{1}{\sigma^2 Re} + i\alpha U \right] \frac{d\tilde{v}_f}{dy} + \frac{1}{Re} \frac{d^3}{dy^3} \left( \frac{\tilde{v}_p}{\varepsilon} - \tilde{v}_f \right) - i\alpha U \tilde{v}_f = 0. \quad (16)$$

The boundary stability equations at the impermeable walls can be given as:

$$\tilde{v}_f = \frac{d\tilde{v}_f}{dy} = 0, \tilde{v}_p = \frac{d\tilde{v}_p}{dy} = 0. \quad (17)$$

The above Eqs. (13) - (17) are the coupled linear instability models in the porous-fluid system, and a spectral collocation method is applied to work out the stability problem.

Here, we present a spectral collocation method based on Chebyshev polynomials and apply it to the Orr-Sommerfeld equation. This method is applied extensively to compute the flow stability characteristics, and is highly accurate. For simplicity, we discuss the case where  $h_f = h_g$ . The problem in the channel region is solved with respect to the axes with origin located on the channel centreline, while the problem in porous region is solved with respect to coordinate system with origins located midway between the interface and the impermeable wall.

We expand the perturbation amplitude functions  $\tilde{v}_f$  and  $\tilde{v}_p$  in Chebyshev series,

$$\tilde{v}_f(y) = \sum_{n=0}^N a_n T_n(y), \tilde{v}_p(y) = \sum_{n=0}^N e_n T_n(y). \quad (18)$$

The derivatives of  $\tilde{v}_f$  and  $\tilde{v}_p$  are obtained by differentiating the above expansions, for example, the second derivatives of  $\tilde{v}_f$  and  $\tilde{v}_p$  are

$$D^2\tilde{v}_f(y) = \sum_{n=0}^N a_n T_n''(y), D^2\tilde{v}_p(y) = \sum_{n=0}^N e_n T_n''(y) \quad (19)$$

and similarly for the fourth derivative, then we make above equations satisfy the Orr-Sommerfeld Eqs. (13) and (14) at the Gauss-Lobatto collocation points  $y_j = \cos(j\pi/N)$ , where  $j = 0, \dots, N$ . Thus, two generalized eigenvalue problems are formed

$$\mathbf{A}\mathbf{a} = \mathbf{c}\mathbf{B}\mathbf{a}, \mathbf{E}\mathbf{e} = \mathbf{c}^2\mathbf{B}\mathbf{e} \quad (20)$$

and the compound matrix equation for the eigenvalue  $c$  and the eigenvectors  $\mathbf{a}$  and  $\mathbf{e}$  is

$$\begin{pmatrix} \mathbf{A} & \mathbf{0} \\ \mathbf{0} & \mathbf{E} \end{pmatrix} \begin{pmatrix} \mathbf{a} \\ \mathbf{e} \end{pmatrix} = c \begin{pmatrix} \mathbf{B} & \mathbf{0} \\ \mathbf{0} & \sigma^2 \mathbf{B} \end{pmatrix} \begin{pmatrix} \mathbf{a} \\ \mathbf{e} \end{pmatrix}. \quad (21)$$

The above Chebyshev series (18) and (19) are also satisfied the boundary stability Eqs. (15)-(17) and then obtained eight boundary conditions are imposed by using eight rows of the compound matrix Eq. (21). The generalized eigenvalue problem can now be worked out following the procedure by [Schmid and Henningson \(2001\)](#).

### 3. COUPLED STABILITY ANALYSES

The coupled linear instability problem of a Poiseuille flow passing through a channel with a porous layer at the bottom is shown in this part. To investigate the impact of interface momentum distribution, we first present the linearized instability analysis at the interface stress coefficient  $\tau = 0$ , and then, we present the stability analysis by varying the interface stress coefficient  $\tau$  from -1.0 to 1.5, since the value of the interface stress coefficient  $\tau$  should be decided by the experiment due to different porous surface characteristics.

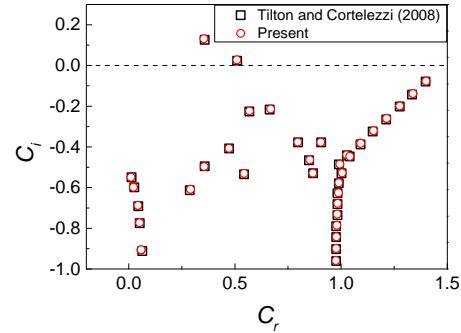


**Fig. 4. Eigenvalues at  $Re = 3000$ ,  $\sigma = 0.02$ ,  $\varepsilon = 0.6$ ,  $\tau = 0.0$ ,  $\alpha = 1.0$ ,  $h_p = 0.25h_f$  for a channel with the lower and upper porous layers.**

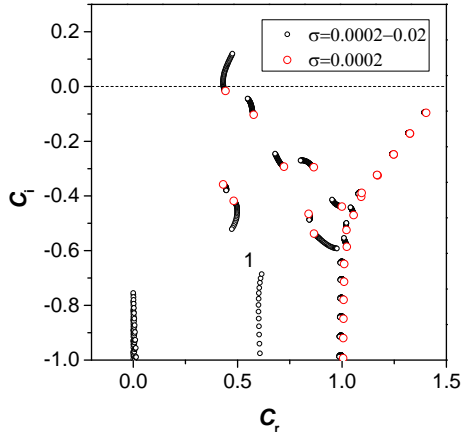
#### 3.1 Validation

Figure 4 shows the comparison the eigenvalues of this study and the study performed by [Tilton and Cortelezzi \(2008\)](#) with the considered parameters  $\sigma = 0.02$ ,  $Re = 3000$ ,  $\varepsilon = 0.6$ ,  $\tau = 0.0$ ,  $\alpha = 1.0$ ,  $h_p = 0.25 h_f$ . A good agreement is observed between these solutions, indicating that the calculated results of this study are credible.

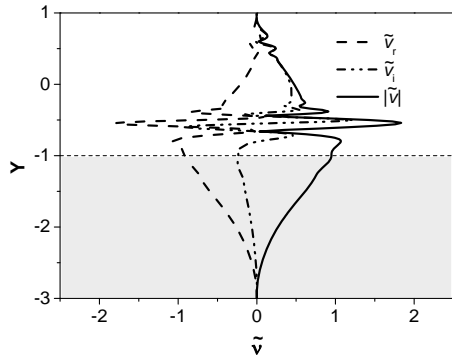
#### 3.2 For the Interface Momentum Distribution Coefficient $\tau = 0$

Figure 5 shows the movement of the eigenvalues in the Orr-Sommerfeld spectrum with increasing the permeability from 0.0002 to 0.02 for  $Re = 2000$ ,  $\varepsilon = 0.6$ ,  $\tau = 0.0$ ,  $h_f/h_p = 1.0$ . It is observed that three branches of circled eigenvalues are located in Fig. 4 called wall modes, porous modes and centre modes as referred to [Tilton and Cortelezzi \(2006\)](#) earlier. Although the locations of these eigenvalues have an overall similar with the results of [Tilton and Cortelezzi \(2006\)](#) and [Li et al. \(2014\)](#), the numbers and the trajectories of the all wall modes (including upper and lower wall modes) are indeed different under a same parameters condition for  $Re = 2000$ ,  $\varepsilon = 0.6$ ,  $\tau = 0.0$ ,  $h_f/h_p = 1.0$ ,  $\sigma = 0.0002-0.02$ . [Tilton and Cortelezzi \(2006\)](#) investigated the flow instability analysis considering a channel having two porous walls on the both sides. They observed that as increasing the permeability, the upper wall modes had only one path line and the two new lower wall modes were induced. However, [Li et al. \(2014\)](#) analyzed the stability results of a channel

inserted one layer porous medium at the centre. They found that with increasing the permeability, the upper wall modes had but two path lines, and two new lower wall modes were also induced. With our present studied channel having only one porous wall at the bottom, note that when increasing  $\sigma = 0.0002-0.02$ , the upper wall modes had only one path line, and only one new lower wall mode labeled 1 is induced in Fig. 5. The perturbation of this mode labeled 1 is shown in Fig. 6, and note that the perturbations near the interface have a higher frequency oscillation.



**Fig. 5. Trajectory of the eigenvalues by varying  $\sigma = 0.0002 - 0.02$  when  $Re = 2000$ ,  $\epsilon = 0.6$ ,  $\tau = 0.0$ ,  $h/h_p = 1.0$ .**



**Fig. 6. Perturbation of the mode labeled 1 for  $Re=2000$ ,  $\sigma = 0.02$ ,  $\tau = 0.0$ ,  $\epsilon = 0.6$ ,  $h/h_p = 1.0$ .**

One of the possible reasons for the different numbers and the trajectories of the wall modes is the different studied geometries of the channels. Since the movements of the wall modes absolutely are affected by the interfaces characteristics, not only the number of porous layers of the channel, but also the location of porous layers can result in the different interfaces characteristics. It shows that based on the present geometry, if increasing one porous wall up of the channel, to be the channel having two porous walls, will make only the number of the upper wall modes increase one; while if changing the location of the porous layer from the bottom of the channel to the middle of the channel, the number of the upper and lower wall modes will

both increase one. Also note that there are little variations of the porous modes or the centre modes whether to change the position or the number of the porous layer.

### 3.3 For the Interface Momentum Distribution Coefficient $\tau = -1.0-1.5$

If the interface momentum distribution impact on the flow instability of the current channel needs to be further investigated, we give the simulation results for the interface stress coefficient,  $\tau$ , in the range of  $\tau = -1.0-1.5$  as following, which contains the continuity and dis-continuity effects of the interface momentum distribution.

Figure 7 shows the results of the eigenvalues trajectory by varying  $\tau = -1.0 - 1.5$  holding the constant  $Re = 2000$ ,  $\epsilon = 0.6$ ,  $\sigma = 0.02$ ,  $h/h_p = 1.0$ . Figure 8 is the corresponding results under the same parameters but  $Re = 3000$ . Note that both in Figs. 7 and 8, changing the interface momentum distribution coefficient from  $-1.0$  to  $1.5$ , significantly may affect the trajectories of the wall modes, especially the most unstable mode of the lower wall modes. It can be seen that these wall modes have obvious movements on the spectrum by varying  $\tau = -1.0 - 1.5$ , but when the coefficient  $\tau$  changes from  $-1.0$  to  $0.0$ , the trajectories of these modes are more obvious than the corresponding situation that when the coefficient  $\tau$  increases from  $0.0$  to  $1.5$ , the locations of these modes vary very small or almost no change. This is just consistent with the conclusion obtained from the above Fig. 3, namely basic flow solution by varying the coefficient  $\tau$  from  $-1.0$  to  $0.0$  shows an even more obvious difference than the situation by increasing the coefficient  $\tau$  from  $0.0$  to  $1.5$ . It can be further considered that in the range  $\tau = -1.0-0.0$ , the interface momentum distribution have a larger effect on the trajectory of the eigenvalues in Orr-Sommerfeld spectrum. In addition, it is interesting to observe that there are two modes labeled 1 and 1' in Fig. 7 (a) and Fig. 8 (a) respectively can never get the results of  $\tau = 0.0$ , and as the coefficient  $\tau$  varies from  $-1.0$  to  $1.5$ , the two labeled wall modes both move facing to their respective porous modes, but finally arrive at different distribution locations.

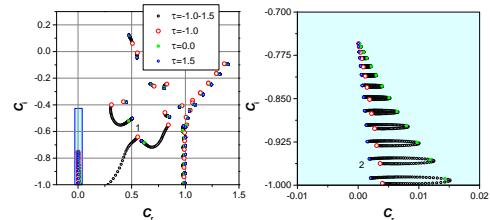


**Fig.7. (a) Trajectory of the eigenvalues by varying  $\tau = -1.0$  (circled) - 1.5 when  $Re = 2000$ ,  $\epsilon = 0.6$ ,  $\sigma = 0.02$ ,  $h/h_p = 1.0$  (b) A larger version of porous modes.**

For the porous modes surrounded by a rectangular in Fig. 7 (a) and Fig. 8 (a) respectively, we see that as  $Re$  increases, the quantity of the porous modes increases, and the porous mode having a maximum

value of the imaginary part of phase speed,  $c_i$ , gets larger. However, as the coefficient  $\tau$  increases, the quantity of the porous modes keeps the same, and the locations seem little or no change both in Fig. 7 (a) and Fig. 8 (a) which differ with the wall modes above mentioned. To observe clearly, we make Figs. 7 (b) and 8 (b) which are the larger version of these porous modes in Figs. 7 (a) and 8 (a). It can be observed that in Fig. 7 (b), each porous mode has an overall upward movement as increasing the value of  $\tau$ , while in Fig. 8 (b), on the contrary, each porous mode overall moves downward. In addition, the porous modes in Figs. 7 (b) and 8 (b) also share a certain same characteristic. That is the porous mode would overlap and may hard to be distinguished visually as the coefficient  $\tau$  varies from -1.0 to 1.5.

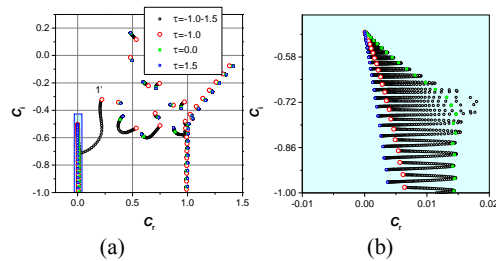
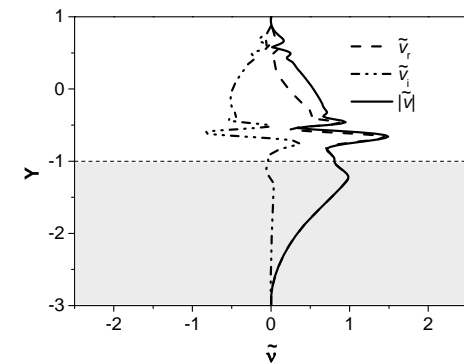
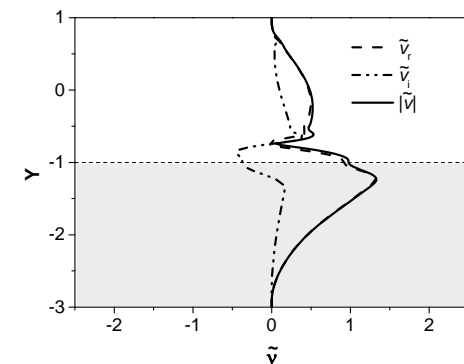


**Fig. 8. (a) Trajectory of the eigenvalues by varying  $\tau = -1.0$  (circled) - 1.5 when  $Re = 3000$ ,  $\varepsilon = 0.6$ ,  $\sigma = 0.02$ ,  $h_f/h_p = 1.0$  (b) A larger version of porous modes.**

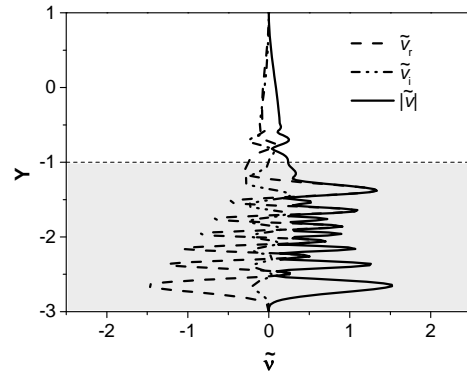


(a) Labeled 1 at  $\tau = -1$  in Fig.7

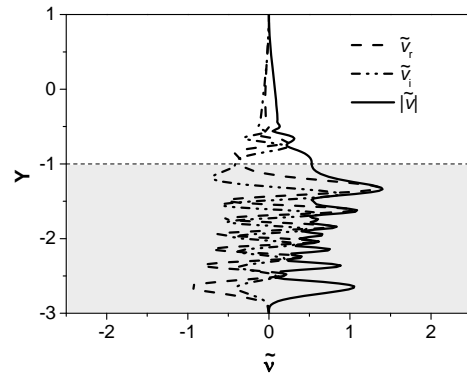


(b) Labeled 1' at  $\tau = -1$  in Fig.8 (a)

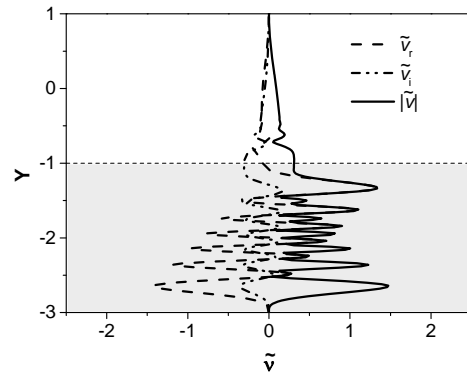
**Fig. 9. Perturbations of the labeled wall modes at different  $Re$ .**



(a) At  $\tau = -1$



(b) At  $\tau = 0$



(c) At  $\tau = 1.5$

**Fig. 10. Perturbations of the labeled 2 modes in Fig.7 (b).**

Figure 9 further illustrates the perturbations,  $\tilde{v}_r$  (dashed line),  $\tilde{v}_i$  (dotted line),  $|\tilde{v}|$  (solid line), of the wall modes labeled 1 and 1' at  $\tau = -1$  (red circled), the trajectories of which can never get the results of  $\tau = 0.0$  in Fig. 7 (a) and Fig. 8 (a) at different  $Re$ . We note that the amplitudes of the perturbations in Fig. 9 (a) occur near two kinds of interface, one is between a fluid layer and a porous wall (permeability wall), the other is between the fluid layer and the impermeability wall. But the perturbation in Fig. 9 (b) near the interface which is between the impermeable wall and the free fluid region hardly can be seen, and the oscillation

frequency of the perturbation near the interface which is between the free fluid region and porous region has an obvious decrement in comparison with that situation in Fig. 9 (a).

Figure 10 illustrates the perturbations,  $\tilde{v}_i$  (dashed line),  $\tilde{v}_i$  (dotted line),  $|\tilde{v}|$  (solid line), of the porous modes labeled 2 at  $\tau = -1, 0, 1.5$  in Fig. 7 (b). Note that these perturbations occur both in the porous region and also near the interface between the porous domain and the free fluid domain. These modes' perturbations in the porous region oscillate at a higher frequency than that near the interface which can be ignored with respect to the perturbations in porous region. Comparing with the examples of  $\tau = -1$  and  $\tau = 1.5$ , the amplitude of the perturbation velocity at  $\tau = 0$  in porous region has a reduction trend, but has an increase near the interface.

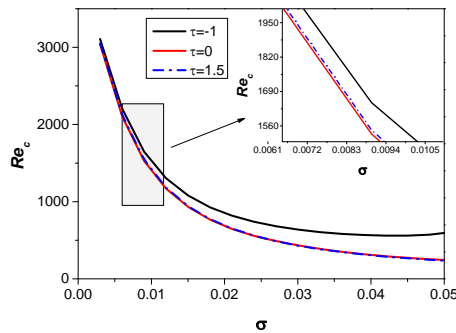


**Fig. 11. The relationships between  $\sigma$  and  $Re_c$  under different  $\tau$  conditions.**

To obtain more insight into how the flow instability is affected by different values of interface momentum distribution coefficient,  $\tau$ , we depict such figure as Fig. 11. Figure 11 indicates the behavior of critical Reynolds number,  $Re_c$ , against permeability,  $\sigma$ , at constant  $\varepsilon = 0.6$ ,  $h_f/h_p = 1.0$  for  $\tau = -1, 0, 1.5$ . In Fig. 11, with the increase of permeability, the value of  $Re_c$  decreases whatever the value of  $\tau$  is. The critical Reynolds number under a small permeability is sensitive and a remarkable drop can be observed, and if the value of permeability is small enough, the value of critical Reynolds number almost overlap together under the three different  $\tau$  conditions. However, when the permeability begins to increase, the value of  $Re_c$  for  $\tau = -1$  becomes greater than the other two cases that  $\tau = 0$  and  $\tau = 1.5$ , and the growth degree may further increase by increasing the permeability. The phenomenon is similar with the situations which is little differences existing for the basic flow and the trajectories of the eigenvalues between  $\tau = 0$  and  $\tau = 1.5$ . But when we enlarge certain regions of the two curves for  $\tau = 0$  and  $\tau = 1.5$ , find that the critical Reynolds number for  $\tau = 1.5$  is slightly greater than the situation for  $\tau = 0$ . Above all, it indicates that, for a channel with a bottom porous medium having a low permeability, the interface momentum distribution has less effect on the flow stability.

While further increasing the permeability, the interface momentum distribution begins to influence the flow stability, especially when  $\tau = -1$ , in which case the fluid passing through the present channel owns the greatest stability, and the fluid stability for  $\tau = 1.5$  is slightly better than the situation of  $\tau = 0$ . For the decrease in critical Reynolds number with increasing  $\tau$  at a fixed permeability  $\sigma$ , one possible explanation is the decrease in interface velocity as increasing  $\tau$ , which can be seen in Fig.3 showing the variations of interface velocity with changing  $\tau$ .

#### 4. CONCLUSION

The effect of the interface momentum distribution (including stress continuity and jump interface conditions) was investigated using spectral collocation method on the stability of Poiseuille flow for a channel partially obstructed by a permeable porous layer on its bottom plate. In order to investigate the effect of the interface characteristics on the stability picture of the main flow, we first present linearized instability results for an interface stress coefficient of  $\tau = 0$  which corresponds to stress continuity at the interface. To study the jump effect of the interface momentum distribution, we then present linearized stability results by changing the interface momentum distribution coefficient,  $\tau$ .

It is predicted that the interface momentum distribution in a negative range has a larger effect on the trajectory of the eigenvalues than that in the positive range, especially on the trajectory of the most unstable mode of the upper wall modes and the lower wall modes. Moreover, with a low permeability in the porous region, the interface momentum distribution has less effect on the main flow stability, while further increasing the permeability, the interface momentum distribution begins to influence the flow stability, especially at  $\tau = -1$ , in which case the fluid flow passing through the present channel owns the greatest stability, but the fluid stability degree for the interface momentum distribution varying in a positive range is slightly to be distinguished from that stress continuity interface condition.

#### ACKNOWLEDGEMENTS

This work was supported by the National Natural Science Foundation of China (Grant No. 41702250 and No.51906034) and the Science and Technology Research Project of Education Department of Jilin Province of China during the "13th Five-Year Plan" (No. JJKH20190701KJ).

#### APPENDIX: THE LAMINAR VELOCITY PROFILE

The determination of constant coefficients  $c_1, c_2, c_3, c_4$  in Eqs.s (9) and (10) is given as follows for laminar velocity profile in the porous-fluid channel. To obtain coefficient values, we first make  $AC^* =$

B by assembling the boundary and interface conditions (7) and (8), then the matrixes as follows can be obtained.

$$A = \begin{pmatrix} 1 & 1 & 0 & 0 \\ -1 & 1 & -a & -b \\ -1 - \tau/\sigma & \tau/\sigma & \frac{a}{\sqrt{\varepsilon}\sigma} & \frac{-b}{\sqrt{\varepsilon}\sigma} \\ 0 & 0 & b & a \end{pmatrix}$$

$$B = (-1 \quad -1 - \sigma^2 \quad -2 - \tau/\sigma \quad \sigma^2)^T$$

where  $a = \frac{\sqrt{\varepsilon}}{\sigma} \cdot \frac{h_p}{h_f}$ ,  $b = -\frac{\sqrt{\varepsilon}}{\sigma} \cdot \frac{h_p}{h_f}$ . From matrixes

A and B, we can obtain the matrix of  $C^* = (c_1^*, c_2^*, c_3^*, c_4^*)^T$  with  $C^* = A^{-1}B$ . Finally the constant coefficients

$$c_1 = c_1^*, c_2 = c_2^*, c_3 = \frac{c_3^*}{1/3 + c_2}, c_4 = \frac{c_4^*}{1/3 + c_2} \text{ in}$$

Eqs. (9) and (10) can be achieved, and these constant coefficients  $c_1, c_2, c_3, c_4$  vary by substituting different parameters.

## REFERENCES

- Avramenko, A. A., A. V. Kuznetsov, B. I. Basok and D. G. Blinov (2005). Investigation of stability of a laminar flow in a parallel-plate channel filled with a fluid saturated porous medium. *Physics of Fluids* 17(9), 094102.
- Barletta, A. (2016). Instability of stationary two-dimensional mixed convection across a vertical porous layer. *Physics of Fluids* 28(1), 014101
- Beavers, G. S., D. D. Joseph (1967). Boundary conditions at a naturally permeable wall. *Journal of Fluid Mechanics* 30, 197-207.
- Beavers, G. S., E. M. Sparrow, D. E. Rodenz (1973). Influence of Bed Size on the Flow Characteristics and Porosity of Randomly Packed Beds of Spheres. *Journal of Applied Mechanics* 40(3), 655-660.
- Berkowitz, B (2002). Characterizing flow and transport in fractured geological media: A review. *Advances in Water Resources* 25(8), 861-884.
- Chang, M., F. Chen, B. Straughan (2006). Instability of Poiseuille flow in a fluid overlying a porous layer. *Journal of Fluid Mechanics* 564, 287-303.
- Coronado, M. and Jetzabeth J. Ramirez-Sabag (2008). Analytical model for tracer transport in reservoirs having a conductive geological fault. *Journal of Petroleum Science & Engineering* 62(3-4), 73-79.
- Dai, C., Q. Li, H. Lei (2015). Instability of Poiseuille flow in a channel filled with multilayer porous media. *Journal of Porous Media* 18, 165-177.
- Hanspal, N. S., A. N. Waghode, V. Nassehi and R. J. Wakeman (2006). Numerical Analysis of Coupled Stokes/Darcy Flows in Industrial Filtrations. *Transport in Porous Media* 64(1), 73-101.
- Li, Q., H. Y. Lei, C. S. Dai (2014). Linear stability of a fluid channel with a porous layer in the center. *Acta Mechanica Sinica* 30, 28-36.
- Liu, R., Q. S. Liu, S. C. Zhao (2008). Instability of plane Poiseuille flow in a fluid-porous system. *Physics of Fluids* 20(10), 104105.
- Ma, M., J. Lu, G. Tryggvason (2016). Using statistical learning to close two-fluid multiphase flow equations for bubbly flows in vertical channels. *International Journal of Multiphase Flow* 85, 336-347.
- Neale, G., W. Nader (1974). Practical significance of Brinkman's extension of Darcy's law: coupled parallel flows within a channel and a bounding porous medium. *The Canadian Journal of Chemical Engineering* 52, 475-478.
- Ochoa-Tapia, J. A. S. Whitaker (1995b). Momentum transfer at the boundary between a porous medium and a homogeneous fluid II. Comparison with experiment. *International Journal of Heat Mass Transfer* 38, 2647-2655.
- Ochoa-Tapia, J. A., S. Whitaker (1995a). Momentum transfer at the boundary between a porous medium and a homogeneous fluid I: theoretical development. *International Journal of Heat Mass Transfer* 38, 2635-2646.
- Pirasteh, G., R. Saidur, S. M. A. Rahman and N. A. Rahim (2014). A review on development of solar drying applications. *Renewable & Sustainable Energy Reviews* 31(2), 133-148.
- Rosti, M. E., L. Cortelezzi, M. Quadrio (2015). Direct numerical simulation of turbulent channel flow over porous walls. *Journal of Fluid Mechanics* 784, 396-442.
- Schmid, P. J., D. S. Henningson (2001). Stability and transition in shear flows. Springer.
- Singh, S., P. Dhiman (2016). Thermal performance of double pass packed bed solar air heaters – A comprehensive review. *Renewable and Sustainable Energy Reviews* 53:1010-1031.
- Tilton, N., L. Cortelezzi (2008). Linear stability analysis of pressure-driven flows in channels with porous walls. *Journal of Fluid Mechanics* 604, 411-455.
- Tilton, N., L. Cortelezzi (2006). The destabilizing effects of wall permeability in channel flows: A linear stability analysis. *Physics of Fluids* 18, 051702.
- Tryggvason, G., M. Ma, J. Lu (2016). DNS-Assisted Modeling of Bubbly Flows in Vertical Channels. *Nuclear Science and Engineering* 184(3), 312-320.

Vafai, K., S. J. Kim (1990). Fluid mechanics of the interface region between a porous medium and a fluid layer—an exact solution. *International Journal of Heat and Fluid Flow* 11, 254-256.

Wedin, H., S. Cherubini (2016). Permeability models affecting nonlinear stability in the asymptotic suction boundary layer: the

Forchheimer versus the Darcy model. *Fluid Dynamics Research* 48(6), 061411.

Whitaker, S. (1996). The Forchheimer equation: A theoretical development. *Transport in Porous Media* 25, 27-61.